SCIENTIA
IRANICA

Research Note

Introducing a New Definition Towards Clinical Detection of Microvascular Changes Using Diffusion and Perfusion MRI

M. Ashoor[1,2], Q. Jiang[2,3], M. Chopp[3,2] and M. Jahed*

Based on MRI diffusion and perfusion, a new criterion for detection and the healing progress of damaged tissue is suggested. The study is based on the ratio of capillary radii in symmetrical damaged and normal tissue neighboring spaces. The Apparent Diffusion Coefficient (ADC) and Cerebral Blood Flow (CBF) were measured in the brain tissues of six male Wistar rats utilizing suggested MRI measurement techniques. The ADC values of damaged and normal regions were $(392 \pm 34.1) \times 10^{-6}$ mm^{2}s^{-1} and $(659 \pm 40.7) \times 10^{-6}$ mm^{2}s^{-1}, respectively. The CBF values of damaged and normal regions were 14.5 ± 10.13 ml/min/100 g and 125 ± 41.03 ml/min/100 g, respectively. The geometrical parameters of the capillary for damaged and normal regions, $\overline{r}/\sqrt{\overline{\ell}}$, where $\overline{r}$ is the mean radius and $\overline{\ell}$ is the mean capillary segment length, were calculated to be 5.45 ± 2.01mm$^{0.5}$g$^{-0.5}$ (mean $\pm$ SD) and 12.8 ± 2.04 mm$^{0.5}$g$^{-0.5}$, respectively. Furthermore, based on constant $\overline{\ell}$, the damaged, versus normal region, mean radius, was shown to follow the "criterion": $\overline{r}_{\text{Damaged}} \cong 0.43 \times \overline{r}_{\text{Normal}}$. A further analysis was conducted through suitable theoretical modeling and assumptions for the above-mentioned criterion. The analysis showed a distinct difference between normal and damaged tissues in various healing progress conditions. Moreover, a new image, namely, Diffusion/Flow map (DF map), which is a mere division of the ADC map to the CBF map, was introduced and utilized to contrast between normal and damaged tissue.

INTRODUCTION

Incoherent microscopic proton motion in vivo is primarily due to diffusion, but, in principle this motion reflects all transport processes within the different tissue compartments, hence, the name Apparent Diffusion Coefficient (ADC). ADC, a measure of the mean free path of water, is consistently reduced in ischemic brain areas in acute strokes. However, the acute pathophysiological mechanisms involved in this phenomenon are not completely understood. Recent studies suggest that ischemia, i.e., interruption of Cerebral Blood Flow (CBF) per se and the resultant brain tissue hypothermia, may cause part of the ADC

reduction. The importance of ADC and its relation to ischemic tissue has previously been extensively studied [1].

Diffusion Weighted magnetic resonance Imaging (DWI) appears useful for the early detection of a stroke. The Apparent Diffusion Coefficient of water (ADCw) predicts cerebral ischemic cell damage, but such prediction is dependent on the time of measurement and duration of ischemia. The ability of a single ADCw measurement to identify and predict the biological outcome of tissue appears linked to a narrow time window requiring precise knowledge of the onset of ischemia. Energy depletion, temperature, intracellular water accumulation, changes in tortuosity of the extracellular diffusion paths and changes in cell membrane permeability have all been implicated as contributing to the changes in ADCw. The increase in ADCw appears to occur concomitantly with a loss of membrane structure and a loss of barriers to diffusion. Possibly, other MRI measurements, such as CBF, phosphorus and proton spectroscopy or a combinations

1. *Department of Mechanical Engineering, Sharif University of Technology, Tehran, Iran.*
2. *Department of Neurology, Henry Ford Health Sciences Center, Detroit, MI, USA.*
3. *Department of Physics, Oakland University, Rochester, MI, USA.*
*. *Corresponding Author, Department of Electrical Engineering, Sharif University of Technology, Tehran, Iran.*

of these measures, may improve tissue characterization [2].

Using a model of the partial stenosis of a Middle Cerebral Artery (MCA) in a cat's brain, Roberts et al. [3] found a linear correlation between relative perfusion reduction and ADC change. In this model, a reduction of CBF correlated well with a reduction in ADC. However, it can be argued that in reperfused infarct, or, when ADC "pseudo-normalizes", the correlation may disappear.

Blood perfusion of tissue assures the delivery of oxygen and nutrients to cells. To achieve this goal, fresh, oxygenated "arterial" blood is delivered to the tissue through the capillary network, which is optimized for blood-tissue exchange. Oxygen and nutrients are transported, passively or actively, in the tissue through the capillary wall. Tissue metabolism results in waste products that are eliminated through the capillary network to constitute deoxygenated "venous" blood. This process depends on many parameters, such as blood pressure and velocity, capillary network density and geometry, capillary wall permeability, nutrient or oxygen diffusion and extraction rates, which can be grouped in three categories: Micro-vascular anatomy and histology, blood microcirculation and blood-tissue exchanges.

For the physiologist, perfusion refers to the circulation of blood. Perfusion has often been used by pathologists (and radiologists) simply to denote the degree (density) of normal or abnormal microvasculature in a tissue, as seen, for instance, by conventional catheter angiography. One should remain cautious regarding the inclusion of "unused" blood in the measured blood flow. In particular, it is known from Positron Emission Tomography (PET) studies that a significant part of circulating blood may come from vessels other than capillaries, such as small arteries and post-capillary veins. Most models assume, for simplicity, that these vessels are "invisible," which could lead to an overestimation of perfusion. The average blood velocity and mean capillary segment length may provide useful data for microcirculation physiology. For instance, when blood flow increases in a particular region of the brain as a response to a sensory stimulus, the physiologist is interested to know whether the mechanism is capillary recruitment or an increase in blood velocity [4].

It may be that combined CBF and ADC can define different acute infarct patterns, which may allow the selection of rational therapeutic strategies, based on the presence or absence of potentially salvageable ischemic tissue. Combined Perfusion-Weighted Imaging (PWI) and Diffusion-Weighted Imaging (DWI) have the potential to be more powerful than either studies alone in predicting infarct outcome. The combination of PWI and DWI was superior to conventional Magnetic Resonance Imaging (MRI) in predicting improvement following severe acute stroke. The acute regional perfusion deficits would correlate with clinical severity, clinical outcome and final infarct size. The combined use of PWI and DWI would be more powerful than either of them alone at identifying patterns in which ischemic regions have the potential to expand [5].

At present, the relationship between capillary geometry and perfusion and diffusion information, such as CBF and ADC, is not fully clear. The combination of CBF and ADC may allow a descriptive statistic related to micro-vascular geometry. A different approach to estimating micro-vascular characteristics can be found in a DF map, which is a mere division of the ADC map to the CBF map. It will be demonstrated, with a preliminary function using CBF and ADC, along with a small set of suitable hypotheses, that the combination of CBF and ADC allows a new descriptive statistic related to micro-vascular geometry. This paper presents a DF map in a rat model of an embolic cerebral ischemic infarction and an interpretation of these maps, in terms of micro-vascular geometry. Micro-vascular parameter changes, after ischemia, are measured.

METHODS

Theory

It is assumed that the number of capillaries, with mean radius, $(n(\overline{r}))$, are maximum and, therefore, the number of capillaries can be calculated as follows:

$$N \cong \int_0^{r_a} n(r)dr \cong (r_a - \overline{r}).n(\overline{r}), \tag{1}$$

where r_a is the maximum radius of capillaries that bring blood into the voxel. If the capillaries are assumed as cylinders with mean length $(\overline{\ell})$ and mean radius $(\overline{r})$, then CBV is as follows:

$$\text{CBV} \cong \int_0^{r_a} n(r).\pi r^2.\ell.dr \cong (r_a - \overline{r})n(\overline{r}).\pi\overline{r}^2.\overline{\ell}. \tag{2}$$

By combining Equations 1 and 2 one obtains:

$$N \cong \text{CBV} \times \left(\pi\overline{\ell}\,\overline{r}^2\right)^{-1}. \tag{3}$$

If TCL is the Total Capillary Length, one has, according to the definition of the Mean Transit Time (MTT) in the capillary network:

$$\text{MTT} = \text{TCL} \times V^{-1} = (\text{TCL}).\overline{\ell} \times (6.D^*)^{-1}$$

$$= \text{CBV} \times \text{CBF}^{-1}. \tag{4}$$

Whereas, before $\bar{l}$ is the mean capillary segment length, defined as the average distance along which spins move with a constant velocity, (V), D^* is the pseudo-diffusion coefficient and CBV is Cerebral Blood Volume [6]. The quantity, $(< \bar{l} >< V > /6)$, has the dimension of a diffusion coefficient and has been referred to as the pseudo-diffusion coefficient, D^*. One may now arrange the cylindrical capillary segments in a series format, namely, $N.\bar{l}$. As such, $N.\bar{l}$ and TCL are practically equal and, hence, by combining Equations 3 and 4, one obtains:

$$\bar{l}.\bar{r}^{-2} \cong 6\pi.D^*.\text{CBF}^{-1}. \tag{5}$$

Using literature data for $< \bar{l} >$ and $< V >$ [7], D^* is expected to be about eight to ten times larger than the true diffusion coefficient of water at room temperature $(D^* \cong 10D)$ [8]. However, currently, a precise measurement of D^* is not possible in view of Signal to Noise Ratio (SNR) limitations. As such, this issue certainly requires further study, especially in the theoretical analysis domain. The authors believe that $D^* \cong 10D$ is a good estimation and starting point for further analytical study and, therefore, it is utilized in the current study. Hence, now based on the above estimation, Equation 5 can be rewritten as:

$$\bar{l}.\bar{r}^{-2} \cong 60\pi.D.\text{CBF}^{-1}. \tag{6}$$

If one assumes that the mean capillary segment length in the capillary space for the normal and damaged regions is the same, one obtains:

$$\bar{r}_{\text{Damaged}} \times (\bar{r}_{\text{Normal}})^{-1} \cong \left((D \div \text{CBF})_{\text{Normal}} \right.$$
$$\left. \times (D \div \text{CBF})_{\text{Damaged}}^{-1} \right)^{0.5}, \tag{7}$$

where $D \div \text{CBF}$ can be regarded as a new image, namely, a DF map. Therefore, the ratio of radii in the damaged and normal regions depends on the ratio of the normal and damaged regions in the DF map.

Animal Model

The male Wistar rats ($N = 6, 300 - 450$ g) subjected to embolic stroke were investigated using a 7 Tesla MRI system. The method of inducing an embolic stroke and the rt-PA treatment in this study has been previously described [9,10]. Briefly, an aged white clot (prepared 24 hrs before ischemia) was slowly injected into the internal carotid artery to block MCA [10]. This model of an embolic stroke provides a relatively reproducible infarct volume localized to the territory supplied by MCA [9,10].

MRI Measurements in 7 Tesla System

MRI measurements were performed using a 7 T, 20 cm bore superconducting magnet (Magnex Scientific, Abingdon, UK) interfaced to a SMIS console (Surrey, England). A 12 cm bore actively shielded gradient coil set, capable of producing magnetic field gradients of up to 20 gauss/cm, was used. Radio Frequency (RF) pulses were applied by a 7.5 cm diameter saddle coil actively decoupled by TTL control from the 1.4 cm surface receiver coil, which was positioned over the center line of the animal skull. Stereotaxic ear bars were used to minimize movement during the imaging procedure. During MRI measurements, anesthesia was maintained using a gas mixture of N_2O (69%), O_2 (30%) and halothane (0.75-1%). Rectal temperature was kept at $37 \pm 0.5°C$, using a feedback controlled water bath. A modified Fast Low Angle SHot (FLASH) [11] imaging sequence was employed for reproducible positioning of the animal in the magnet at each MRI session [12]. DWI and PWI measurements were performed 24 hrs after the onset of embolization.

ADCw was measured using the Stejskal-Tanner sequence with three b-values (10, 800 and 1800 s/mm^2) in each of three diffusion sensitizing directions, seven slices, 32 mm^2 FOV, 128×64 matrix, TR = 1.5 s; TE = 40 ms, where FOV, TR and TE are Field Of View, Repetition Time and Echo Time, respectively. Each image required a scan time of 3.2 min for completion. The total time for the entire sequence was approximately 14.4 min.

Perfusion measurements were performed prior to each diffusion measurement using an arterial spin tagging technique [13]. Two images were obtained for perfusion measurement with parameters: TR = 1 sec, TE = 30 msec, 64×64 image matrix, 3 mm slice thickness and a 32 mm^2 FOV. In each animal, PWI was measured within a coronal section, with coordinates centered at interaural 8.2 mm and bregma 0.8 mm [14]. The duration of the inversion pulse was 1 sec at a B1 amplitude of 0.3 KHz.

Data Analysis

Two Regions Of Interests (ROIs) were selected for measurement of MRI parameters. The mean and Standard Deviations (SD) of ADCw values of the parenchymal tissue (not Cerebrospinal Fluid (CSF)) in the contralateral hemisphere were measured and the threshold values, to determine the number of pixels with abnormal values in the ipsilateral hemisphere, were defined using mean ADCw $-1.5 \times$ SD in the contralateral hemisphere, where this value is a heuristic one. Homologous ROIs in the ischemic tissue were also measured in the contralateral hemisphere. A

paired t-test was used to compare the two ROIs with a significance level of 0.05.

RESULTS

For the calculation of ADC, the mono-exponential intra-voxel incoherent motion model was used: $S(b) = S(0).\exp(-b.\text{ADC})$ [12]. Because the diffusion of water may be directionally dependent (anisotropic), measurement in only one direction can lead to incorrect image interpretation. The diffusion gradient was, therefore, applied in each of three orthogonal directions (x, y, z) and an average of these measurements was calculated to give the trace of the diffusion tensor, which is reported to minimize the effects of diffusion anisotropy [5].

The ADC, CBF and DF images were formed using the above protocols that were identified in Figure 1. In the damaged areas of both the ADC and CBF maps, the values were decreased relative to the normal area because of stroke onset. For calculation of ADC and CBF values, suitable areas are chosen after applying image processing procedures to reduce noise and artifacts. So, the ADC values of damaged and normal regions were $(392 \pm 34.1) \times 10^{-6}$ mm^{2}s^{-1} and $(659 \pm 40.7) \times 10^{-6}$ mm^{2}s^{-1}, respectively. The CBF values of damaged and normal regions were 14.5 ± 10.13 ml/min/100g and 125 ± 41.03 ml/min/100g, respectively. The geometrical parameters of capillaries for damaged and normal regions, $\overline{r}/\sqrt{\overline{\ell}}$, were calculated to be 5.45 ± 2.01 mm$^{0.5}$g$^{-0.5}$ (mean$\pm$ SD) and 12.8 ± 2.04 mm$^{0.5}$g$^{-0.5}$, respectively. Furthermore, based on constant $\overline{\ell}$, damaged versus normal region mean radius was shown to follow the "criterion": $\overline{r}_{\text{Damaged}} \cong 0.43 \times \overline{r}_{\text{Normal}}$.

Table 1 depicts the ADC, CBF and $\overline{r}/\sqrt{\overline{\ell}}$ values. Figure 2 depicts the relationship between mean length and radius in damaged and normal regions. As shown in this figure, the mean radius in the damaged region is less than the normal region and with increasing the mean length, mean radius will be increased. Figure 3 illustrates capillary radius versus ADC and CBF for the mean lengths of 50, 100 and 250 μm in the capillary space. Here, as CBF increases with a low ADC value, the mean capillary radius is rapidly increased. Figure 4 demonstrates capillary length versus ADC and CBF for the mean radius of 2, 3 and 4 μm. It can be
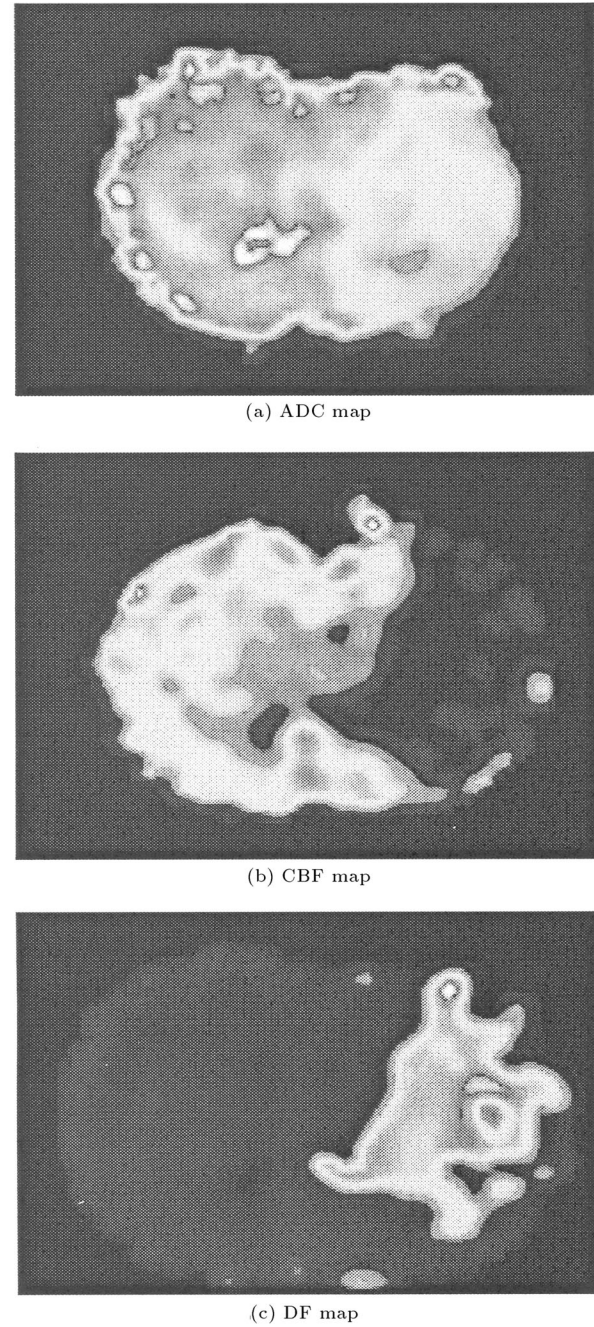

(a) ADC map

(b) CBF map

(c) DF map

Figure 1. a) ADC map depicting normal versus damaged where the latter is shown as a bright segment; b) CBF map for blood flow in the same normal versus damaged area as in part (a); and c) DF map providing the specific damaged area.

Table 1. The ADC, CBF and $\overline{r}/\sqrt{\overline{\ell}}$ values in the damaged and normal regions (presented for the theory of being in agreement with published values (mean $\pm$ SD)).

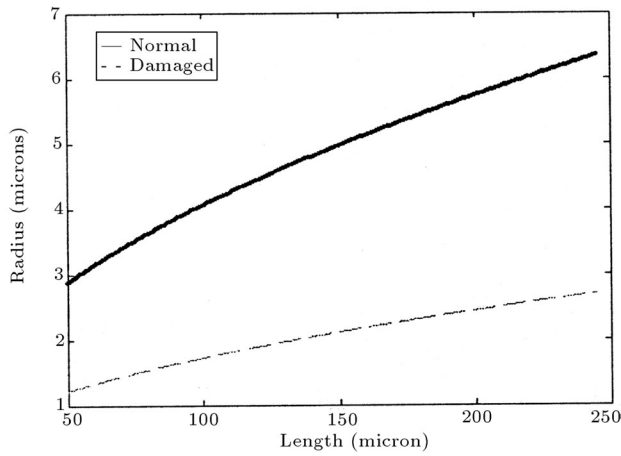|	ADC (mm^2/sec)	CBF (ml/min/100 g)	$\overline{r}/\sqrt{\overline{\ell}}$ mm$^{0.5}$ g$^{-0.5}$
Damaged Region	$3.92 \times 10^{-4} \pm 3.41 \times 10^{-5}$	14.5 ± 10.13	5.45 ± 2.01
Normal Region	$6.59 \times 10^{-4} \pm 4.07 \times 10^{-5}$	125 ± 41.03	12.8 ± 2.04
Damaged to Normal Ratio	0.595 ± 0.04	0.116 ± 0.07	0.4 ± 0.13

**Figure 2.** Relationship between mean length and radius of capillary in damaged and normal regions.

seen that with increasing radius, the length of the capillary will also increase. Moreover, the mean radius in the capillary space dropped off in the damaged regions where perfusion and diffusion values decreased approximately 9 and 2 fold, respectively. For example, considering a mean capillary length of 100 microns, using Equation 6, the mean radius in the capillary space of the damaged and normal areas, was found to be 1.72 and 4.05 microns, respectively.

DISCUSSION

This study provides a new definition for the relationship between the mean radius of the capillary in the damaged and normal regions using diffusion and perfusion MRI. Diffusion, CBF and DF maps are obtained through the application of image processing techniques (e.g. threshold technique) to reject noise.

Ideally, one should consider all requisites for the dynamical modeling of the system, namely, fluid, thermal dynamics and various parameters involved in capillary spaces. However, the emphasis of this study has been to find a simplified method to provide a suitable clinical application criterion, namely, a DF map produced from diffusion and perfusion maps and the ratio of capillary radii in damaged versus normal tissue. The ratio of capillary radii is not as important as a specific quantified number, but, rather, departure from this quantity is important in damaged versus normal cases. As such, one must notice that, although this study elects to overlook a few dynamical system parameters, it has provided a possible resolution towards diagnostics and the prediction of abnormalities.
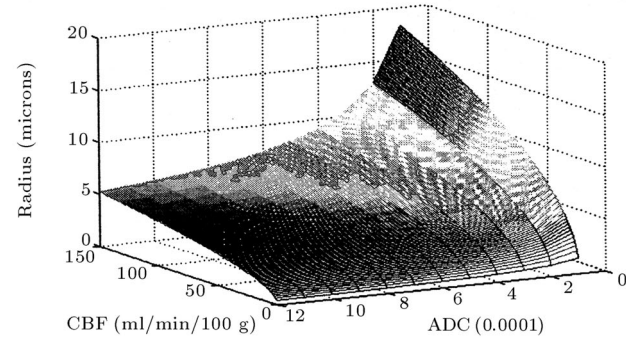
Pathak et al. [15] showed that in normal contralateral sections of the brain, the mean vessel length and radius were, respectively, 178.59 ± 28.76 and 3.72 ± 0.72 microns, while the same parameters for a tumor were 98.36 ± 14.74 and 10.52 ± 2.94 microns, respectively.
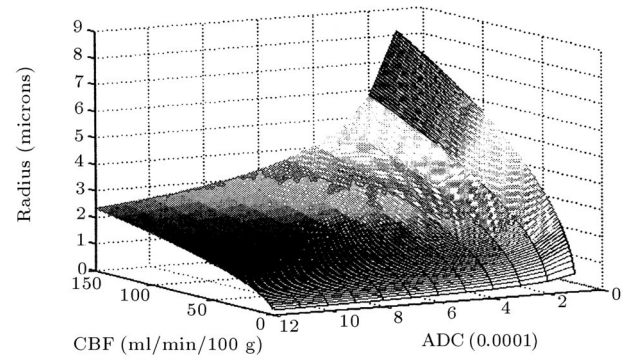
(a) Length = 50 microns
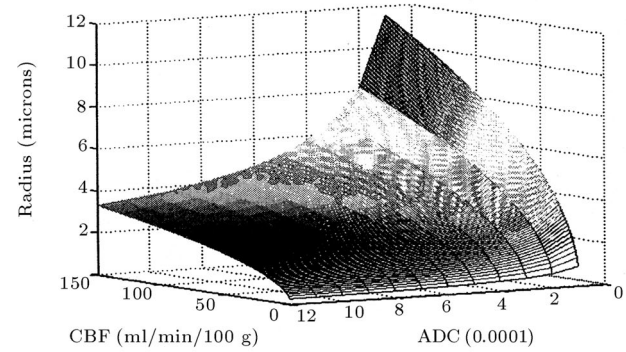
(b) Length = 100 microns

(c) Length = 250 microns

Figure 3. Capillary radius versus ADC and CBF for mean length of a) 50, b) 100 and c) 250 μm. Here, as CBF increases with a low ADC value, the mean capillary radius is rapidly increased.

The ADC measured in this study is, in fact, a weighted average of the diffusion coefficients of the intracellular and interstitial compartments. The diffusion coefficients for two separate compartments, Dint (interstitial) and Din (intracellular), were given in the literature as Dint = 0.00325 mm^{2}s^{-1} and Din = 0.000143 mm^{2}s^{-1}. In a normal brain, the interstitial space volume is 20% of the total volume, whereas the intracellular compartment comprises, approximately, 80% of the total volume. Thus, for a normal brain, one may calculate an average weighted diffusion coefficient of $(0.2 \times 0.00325 + 0.8 \times 0.000143$ mm^{2}s$^{-1})$ or
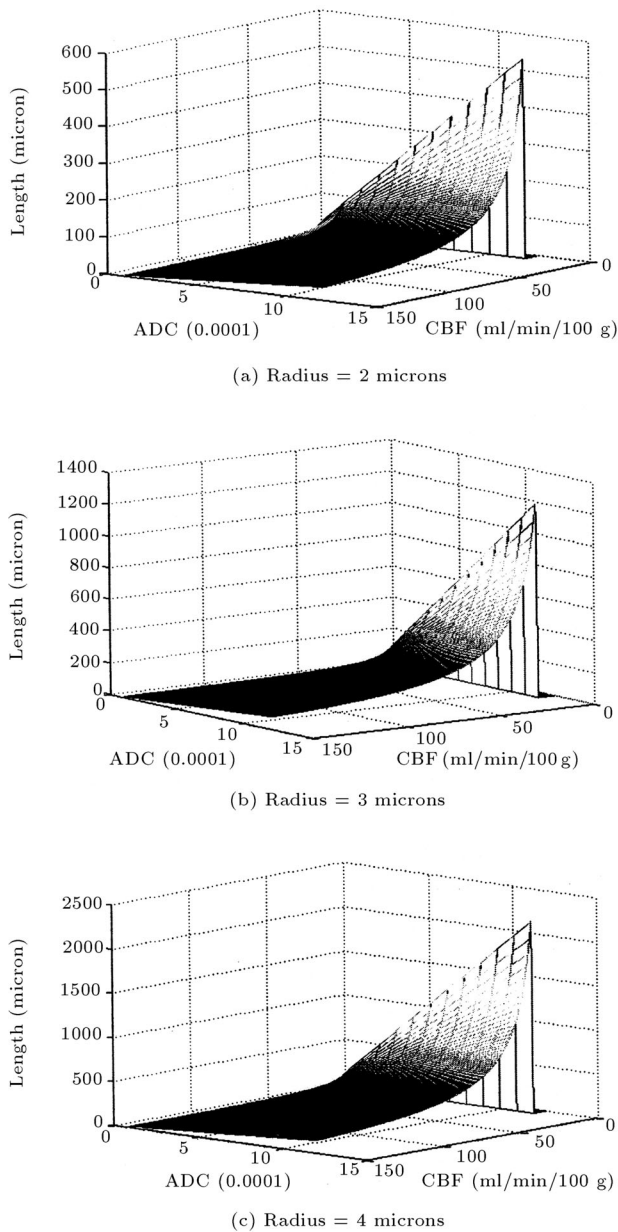
(a) Radius = 2 microns

(b) Radius = 3 microns

(c) Radius = 4 microns

Figure 4. Capillary length versus ADC and CBF for mean radius of a) 2, b) 3 and c) 4 μm.

0.00076 mm^{2}s^{-1} [1]. This, however, is in agreement with the results obtained in this study.

The precise physiologic correlation of D^* to CBF is not exactly known, but this parameter seems most likely related to the velocity of blood through the vessels. As such, it is reasonable that D^* would increase with increasing CBF [16]. Yet, in another study, the pathophysiological changes were shown to be the reasons for the gradual ADC reduction in the ischemic territory. ADC values of normal cortex and caudate-putamen were found to be $(726 \pm 22) \times 10^{-6}$ mm^{2}s^{-1} and $(659 \pm 17) \times 10^{-6}$ mm^{2}s^{-1}, respectively [17]. Again, the measured values are in agreement with these results.

The DF-map shows that the microcirculation effect arises from capillary blood and not from any other circulating fluid, such as CSF in the brain. It seems that the CSF region in the DF-map disappears. The standard deviation of CBF is large. This is likely due to variable biological events, as well as to errors inherent in the spin tagging CBF methodology. Errors in the proton spin tag MRI CBF measurement may derive from the relatively low signal-to-noise ratio (approximately 5:1 for CBF map) [9]. The high S.D. of the observed lesion size reflects the inter-individual variability of the extent of ischemic territory [17].

Advantages of the DF-map in Figure 1 may be summarized as follows:

a) Prevents data scattering in CBF and ADC images;

b) Separates normal and lesion regions;

c) It is not sensitive to simultaneous changes of CBF and ADC. Therefore, regions with small and large CBF and ADC values have similar values in the DF-map. On the other hand, it shows the same results whether CBF and ADC values are low or high;

d) It shows promise in predicating capillary density;

e) In the DF map, the utilization of combined PWI and DWI has the potential to be more powerful than either studies alone in predicting infarct outcome.

On the other hand, the disadvantage of the DF map was, primarily, due to longer experimental time.

Based on the presented results, it may be concluded that lesion volume in the DF map correlates well with clinical indications. In practice, it seems that the DF map can be used to quantify the efficiency of blood flow to deliver oxygen and nutrients to, and waste from, the tissues. Finally, a DF map may find usage in identifying tissue regions at risk for eventual infarctions.

REFERENCES

1. Benveniste, H., Hedlund, L.W. and Johnson, A. "Mechanism of detection of acute cerebral ischemia in rats by diffusion-weighted magnetic resonance microscopy", *Stroke*, **23**, pp 746-754 (1992).

2. Jiang, Q., Chopp, M., Zhang, Z.G., Knight, R.A., Jacobs, M., Windham, J.P., Peck, D., Ewing, J.R. and Welch, K.M.A. "The temporal evolution of MRI tissue signatures after transient middle cerebral artery occlusion in rats", *Journal of Neurological Sciences*, **145**, pp 15-23 (1997).

3. Roberts, T.P.l., Vexler, Z., Derugin, N., Moseley, M.E. and Kucharczyk, J. "High-speed MR imaging of ischemic brain injury following stenosis of the middle cerebral artery", *J. Cerebral Blood Flow Metabolism*, **13**, pp 940-946 (1993).

4. Bihan, D.L. and Turner, R. "The capillary network: A link between IVIM and classical perfusion", *Magnetic Reson. Med. (MRM)*, **27**, pp 171-178 (1992).

5. Barber, P.A., Darby, D.G., Desmond, P.M., Yang, Q., Gerraty, R.P., Jolley, D., Donnan, G.A., Tress, B.M. and Davis, S.M. "Prediction of stroke outcome with echoplanar perfusion- and diffusion-weighted MRI", *Neurology*, **51**, pp 418-426 (1998).

6. Bihan, D.L., *Intravoxel Incoherent Motion Imaging: Diffusion and Perfusion Magnetic Resonance Imaging*, D. Le Bihan, Ed., Raven Press, Ltd., New York, USA, chapter 15, pp 270-274 (1995).

7. Pawlik, G., Rackl, A. and Bing, RJ. "Quantitative capillary topography and blood flow in the cerebral cortex of cats: An in-vivo microscopic study", *Brain Res.*, **208**, pp 35-58 (1981).

8. Bihan, D.L. "Molecular diffusion nuclear magnetic resonance imaging", *Magnetic Reson. Quarterly*, **7**(1), pp 1-30 (1991).

9. Jiang, Q., Zhang, R.L., Zhang, Z.G., Ewing, J.R., Divine, G.W. and Chopp, M. "Diffusion-, T2-, and perfusion-weighted nuclear magnetic resonance imaging of middle cerebral artery embolic stroke and recombinant tissue plasminogen activator intervention in the rat", *J. Cerebral Blood Flow and Metabolism*, **18**, pp 758-767 (1998).

10. Zhang, R., Chopp, M., Zhang, Z., Jiang, Q. and Ewing, J.R. "A rat model of embolic focal cerebral ischemia", *Brain Research*, **766**, pp 83-92 (1997).

11. Haase, A., Frahm, J., Matthaei, D., Hanicke, W. and Merboldt, K.D. "FLASH imaging, rapid NMR imaging using low flip-angle pulses", *Journal of Magnetic Reson.*, **67**, pp 258-266 (1986).

12. Jiang, Q., Zhang, Z.G., Chopp, M., Helpern, J.A., Ordidge, R.J., Garcia, J.H., Marchese, B.A., Qing, Z.X. and Knight, R.A. "Temporal evolution and spatial distribution of the diffusion constant of water in rat brains after transient middle cerebral artery occlusion", *Journal of Neurol. Sci.*, **120**, pp 123-130 (1993).

13. Williams, D., Detre, J., Leigh, J. and Koretsky, A. "Magnetic resonance imaging of perfusion using spin inversion of arterial water", *Proc. National Academy of Sciences*, USA, **89**, pp 212-216 (1992).

14. Paxinos, G. and Watson, C., *The Rat Brain in Stereotaxic Coordinates*, 2nd Edn., Academic Press (1986).

15. Pathak, A.P., Schmainda, K.M., Ward, B.D., Linderman, J.R., Rebro, K.J. and Greene, A.S. "MR-derived cerebral blood volume maps: Issues regarding histological validation and assessment of tumor angiogenesis", *Magnetic Reson. Med. (MRM)*, **46**, pp 735-747 (2001).

16. Neil, J.J., Bosch, C.S. and Ackerman, J.J.H. "An evaluation of the sensitivity of the intravoxel incoherent motion (IVIM) method of blood flow measurement to changes in cerebral blood flow", *Magnetic Reson. Med. (MRM)*, **32**, pp 60-65 (1994).

17. Hoehn-Berlage, M., Norris, D.G., Kohno, K., Mies, G., Leibfritz, D. and Hossmann, K.-A. "Evolution of regional changes in apparent diffusion coefficient during focal ischemia of rat brain: The relationship of quantitative diffusion NMR imaging to reduction in cerebral blood flow and metabolic disturbances", *Journal of Cerebral Blood Flow and Metabolism*, **15**, pp 1002-1011 (1995).